Nanoscale Advances

ROYAL SOCIETY OF CHEMISTRY

COMMUNICATION

View Article Online
View Journal | View Issue

Open Access Article. Published on 05 November 2025. Downloaded on 1/22/2026 5:16:16 PM.
This article is licensed under a Creative Commons Attribution-NonCommercial 3.0 Unported Licence.

Check for updates

Cite this: *Nanoscale Adv.*, 2025, **7**, 7891

Received 2nd September 2025
Accepted 5th November 2025

DOI: 10.1039/d5na00846h

rsc.li/nanoscale-advances

Direct access to the graphene–metal interface using Raman spectroscopy to study the origin of contact resistance in operational devices

Alessandro Kovtun, *[a] Leonardo Martini[b] and Piera Maccagnani*[c]

We present and validate a reliable approach for investigating the graphene–metal interface in the top metallic contacts of operational devices using Raman spectroscopy. A transparent substrate was optimized for graphene visualization and processing by adjusting the thickness of aluminum and amorphous silicon nitride on a glass substrate. After graphene photolithography and Cr/Au contact fabrication, the device was flipped upside down to directly expose the graphene–metal interface for Raman analysis using 457 nm excitation. Electrical characterization was performed on the same devices: the sheet resistance was measured using the van der Pauw method, and the contact resistance was determined using the transfer length method. This approach enables direct correlation between Raman features—an increased D peak and a reduced 2D peak at the graphene–metal interface—and electrical parameters of the contact. In particular, the higher sheet resistance of graphene beneath the metal corresponds to the reduced p-doping obtained using Raman spectroscopy.

Introduction

The contact resistance of graphene/metal interfaces is a crucial parameter that affects the performance of devices based on graphene. High contact resistance can limit the current in graphene-based field effect transistors (GFETs)[1] and is currently the main factor limiting the radio-frequency bandwidth in a graphene phase modulator.[2] The integration and downscaling of graphene electronic devices present an important challenge in the development of a complementary metal-oxide-semiconductor (CMOS) compatible process, which enables the reproducible formation of low contact resistance.[3] Furthermore, interest in contact resistance has led to the standardization of the transfer length method (TLM) to investigate many different metals and combinations of metals on graphene.[4] However, the origin of contact resistance still has space for debate since no direct spectroscopic characterization can be performed on working devices. Most discussions on the fundamental aspects of graphene/metal interfaces are based on DFT results,[5] suggesting that the main mechanism underlying contact resistance arises from the doping effect due to work function (W_F) differences between graphene and the metal, which has been experimentally investigated.[6] However, experimental evidence indicates that contact resistance is strongly related to W_F, while defect induction on graphene by oxygen or plasma treatments seems to affect the devices dramatically[7] as well as the effective surface area of the graphene/metal interface, which may change due to different sizes of metallic granules[8] or the induction of anti-dots in graphene.[9]

Despite the interest in this area, no spectroscopic technique can probe the graphene–metal interface of a TLM device due to the high thickness of the metal used (in the range of several tens of nanometers). In this case, visible light is totally reflected by the metal before reaching the underlying graphene, and the electrons used as probes have an inelastic mean free path that is one or two orders of magnitude shorter than the thickness of the metal. As a result, spectroscopy techniques such as Raman spectroscopy and photoelectron techniques (X-ray and ultraviolet photoelectron spectroscopy, XPS/UPS) are not suitable. For this reason, most studies in the literature on graphene/metal interfaces use a thin metal layer (few nanometers thick) deposited using different techniques, hindering the electrical characterization of the contact resistance. Characterization techniques used on these samples, such as XPS[10] or near-edge X-ray absorption fine structure (NEXAFS),[11] have shown the presence of defects due to the formation of carbide (Carbon–Metal, C–M) covalent bonds and, in some cases, the oxidation of those carbides into carbonates (C=O). Notably, most studies on few nm thick metals on graphene focus on Raman spectroscopy on Ni, Co, Au and Ag,[12] or Cr and Ti,[13] and have reported some

[a]Consiglio Nazionale delle Ricerche, Istituto per la Sintesi Organica e la Fotoreattività, (CNR-ISOF), 40129 Bologna, Italy. E-mail: alessandro.kovtun@cnr.it

[b]Dipartimento di Scienze Fisiche, Informatiche e Matematiche (FIM), Università di Modena e Reggio Emilia, 41125 Modena, Italy

[c]Consiglio Nazionale delle Ricerche, Istituto per lo Studio dei Materiali Nanostrutturati, (CNR-ISMN), 40129 Bologna, Italy. E-mail: piera.maccagnani@cnr.it

© 2025 The Author(s). Published by the Royal Society of Chemistry

Open Access Article. Published on 05 November 2025. Downloaded on 1/22/2026 5:16:16 PM.
This article is licensed under a Creative Commons Attribution-NonCommercial 3.0 Unported Licence.

local spectral modifications, like shifts of 2D and G Raman bands or modification of relative intensities of these peaks. Although these studies cannot correlate contact resistance with structural properties, due to the impracticality of fabricating working devices with such thin contacts, they are extremely useful for understanding the interaction between graphene and metals. In studies involving operational devices with thicker metal contacts (close to 100 nm), Raman spectroscopy has been performed on the edge of the contact area, observing some modifications to the Raman signal.[14] However, no clear correlation between the contact resistance and structural properties has been found. Some studies report the evolution of Raman spectra on graphene films in regions where the contact has been removed.[15] The only graphene/metal interface studied by Raman in operational devices was reported by Sakavičius, and it is based on a bottom contact geometry.[16,17]

In order to overcome the current limitations in studying the graphene/metal interface in operational devices, we propose and validate a reliable approach that can be applied to any top contact fabrication geometry (TLM, 4-point probe, FET, *etc.*). This approach consists of using a transparent substrate for device fabrication, which is compatible with state-of-the-art micro-fabrication technologies. This allows for the creation of functional electrical devices suitable for electrical characterization while also providing direct access to the graphene/metal interface *via* Raman spectroscopy, simply flipping the device upside down, as validated in the present work. A similar approach has been previously exploited by Fromm to investigate graphene grown on SiC,[18] but no dedicated studies on contact are currently reported.

Experimental

Transparent substrate

The substrate was optimized to maintain the optical contrast necessary to visualize the graphene film during the alignment process, similar to that observed with 300 nm SiO_2 on a Si substrate.[19] This is achieved using an amorphous silicon nitride (a-SiN, 212 nm thick) layer on top of a semi-reflecting 7 nm aluminum layer deposited on a glass cover slip with a size of 20 × 20 mm^2 (and referred to as a-SiN/Al/Glass); when graphene is transferred onto it, we can denote it as G/a-SiN/Al/Glass, or more simply as G/a-SiN for graphene with no contact, and Au/Cr/G/SiN for the graphene in the contact region. Aluminum was thermally evaporated in an electron beam Varian 3119 system, while the a-SiN layer was deposited at a low temperature using a plasma-enhanced chemical vapor deposition (PECVD) process on top of the aluminum film. The Raman spectra of graphene on a-SiN can be directly compared with those of graphene on SiO_2.[20] However, for the sake of clarity, we fabricated and characterized the devices on both substrates: graphene on a 300 nm SiO_2/Si wafer (or referred to as G/SiO_2)—the most common substrate, though not suitable for Raman investigation under contact—and graphene on a-SiN. A good compromise between optical contrast and transparency was optimised by tuning the thickness of Al and a-SiN after simulating the transmittance and reflectance curves using the transfer-matrix method (TMM).[21] The optimal substrate provides good contrast for the visualization of graphene due to the significant difference in reflectivity around the 500 nm wavelength (Fig. 1b), and it allows an overall transmittance of *c.a.* 40% Raman measurements using a 457 nm laser.

The graphene structures are obtained starting from a few layer graphene film (FLG), grown by means of a catalytic-CVD process,[22] which is transferred onto the substrate (SiO_2 or a-SiN) using a 1 μm thick poly-methyl-methacrylate polymer (PMMA 950-A7, micro resist technology GmbH, Berlin, Germany) as a supporting layer. After transfer, PMMA was removed in acetone vapors, and graphene was lithographically patterned using an HPR-504 resist and dry etched in oxygen plasma (25% O_2 + 75% N_2). The metal contact on graphene was realized by thermal evaporation of Cr in the electron beam Varian 3119 system, followed by RF sputtering at room temperature in an MRCC 8622 RF system (180 W) of an Au layer and using a lift-off process, where PMMA (exposed in DUV light, 248 nm) was used as the resist.[22] The final contact had 20 nm of chromium (Cr) and 70 nm of gold (Au) (Fig. 1a).

Electrical characterization

The electrical characterization of the graphene/metal contact is performed using the contact-end-resistance (CER) method applied to transfer length method (TLM) structures, as suggested in ref. 23 The fabricated TLM structures have 4 graphene channel widths (5, 10, 20 and 40 μm), while the spacing (L_{CH}) between the contacts ranges from 5 to 50 μm with a 5 μm increase, and the metal line contacts are 6 μm wide. On the same substrate (2 × 2 cm^2), several TLM and Van der Pauw (VdP) devices were fabricated. The cross-section of the metal/graphene TLM and van der Pauw structures is shown in Fig. 1a, while the measurement setup used for the TLM is illustrated in Fig. S1. No back gate voltage was applied to the device (the 212-nm thick a-SiN layer acts as an insulator between the graphene and the underlying aluminum layer). The experimental details of the DC characterization are reported in the SI.

Micro Raman

Each Raman spectrum was obtained by a 5 s acquisition time repeated 10 times; a 457 nm laser and a 100× long working distance objective were used on the Renishaw Invia Qontor Raman spectrometer. The incident laser power on the sample was on the order of 1 mW μm^{-2}. To validate the Raman analysis, the signals of graphene on a-SiN and SiO_2 were acquired in a conventional sample disposition, while the investigation of the graphene–metal interface on the contact was possible by acquiring the Raman signal from a sample with a transparent substrate (a-SiN) in an upside down configuration–glass on top and graphene on bottom. Optical microscope images of the upside down structures are shown in Fig. 1c for the VdP and Fig. 1d for the TLM structures. From this last image, it is possible to note that the indications of the channel width (W20) and the numbers for different channel lengths (10 and 30) are mirrored. The obtained maps were acquired on both TLM (12 ×

 © 2025 The Author(s). Published by the Royal Society of Chemistry

Open Access Article. Published on 05 November 2025. Downloaded on 1/22/2026 5:16:16 PM.
This article is licensed under a Creative Commons Attribution-NonCommercial 3.0 Unported Licence.

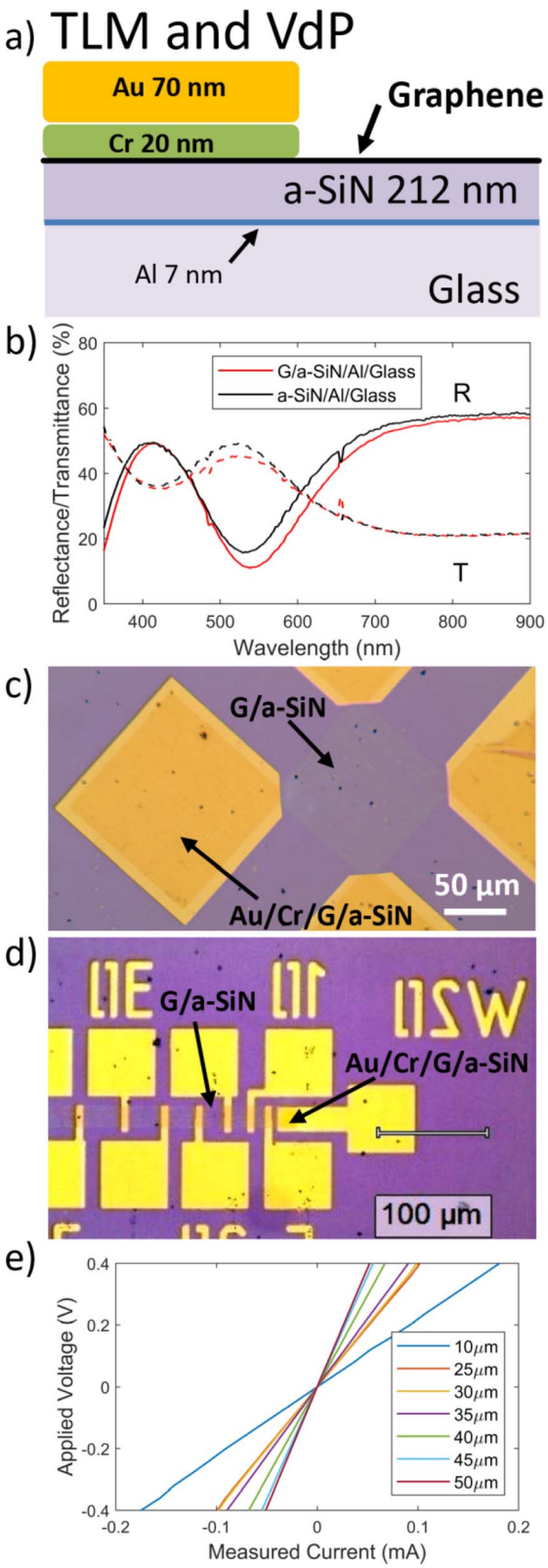

Fig. 1 (a) Scheme of the transparent substrate (a-SiN/Al/Glass), with graphene (G) on top and contacts (Au/Cr) for TLM and VdP test structures; (b) measured transmittance and reflectance for the G/a-SiN/Al/Glass sample. Transferring graphene reduces both transmittance and reflectance of the transparent substrate; (c) microscopy image of VdP from the glass side (upside down); (d) microscopy image of TLM (width of graphene 20 µm) test structure from the glass side (upside down); and (e) I–V curves of graphene contacted with Cr and Au (Au/Cr/G/a-SiN) with the pad distance changing from 10 to 50 µm.

44 µm^2, 2 µm step, 161 points) and VdP (9 × 54 µm^2, 3 µm step, 76 points) structures. The Z focus was optimized at the graphene/metal interface by minimizing the laser spot size on the sample and maintaining it constant throughout the measurement. In contrast to what is suggested by the main guidelines,[24] where the position of focus is further optimized by scanning the Z axis during the acquisition of the Raman signal, in fact, applying this latter approach in the upside down configuration, the focus would move from the graphene/metal interface, broadening the spot size of the laser and obtaining an inaccurate Raman spectrum. The Raman signal was analysed by fitting the D, G, D′ and 2D signals for each spectrum and by combining these parameters to obtain the intensity map for (i) full width at half maximum of 2D signal (FWHM of 2D), (ii) intensity ratio of 2D over G signal (I_{2D}/I_G) and (iii) intensity ratio of D over G (I_D/I_G) using Matlab. The values reported for the D, G, D′ and 2D positions and the relative intensities were obtained by averaging those found for the micro Raman maps.

Results and discussion

This section opens with the electrical characterization results of FLG on both a transparent substrate (G/a-SiN) and a conventional opaque substrate (G/SiO_2), followed by the validation of the Raman analysis of both systems. Finally, the Raman investigation at the graphene–metal interface is presented, and its correlation with electrical measurements is discussed.

By applying a voltage between contacts 1 and 2 (Fig. S1) of the TLM structures, a linear behaviour is observed in all I–V measurements (Fig. 1e), confirming that the total resistance can be obtained by applying the equation $R_T = V_{12}/I_{12}$. Because the sheet resistance of graphene under the metal contact (R_{SK}) is different from that of graphene (R_{SH}), the CER method[25] was used to evaluate R_{SK}; the transfer length (L_{TK}), which represents the active portion of the contact involved in the conduction (typically $L_{TK} < L_{CON}$) and the specific contact resistivity associated with the graphene/metal interface (ρ_C). The graphene sheet resistance, R_{SH}, is obtained from 4-point van der Pauw measurements. More details about the technique used for the extraction of the electrical parameters are reported in the SI.

The main electrical parameters extracted for the two different substrates—G/SiO_2 and G/a-SiN—are summarized in Table 1 (a description of the method used for parameter extraction is reported in the SI). The two samples have similar values for all the main graphene parameters, except for the sheet resistance of graphene under the contact, R_{SK}. In both samples, R_{SK} is higher than the graphene sheet resistance R_{SH}, as expected, due to the interaction of the metal contact with the underlying graphene. Typically, our graphene is p-doped and characterized after transfer by a hole density in the range of 10^{12}–10^{13} cm^{-2}, while the metal is characterized by a large number of electrons in the order of 10^{21}. After the fabrication of

Open Access Article. Published on 05 November 2025. Downloaded on 1/22/2026 5:16:16 PM.
This article is licensed under a Creative Commons Attribution-NonCommercial 3.0 Unported Licence.

Table 1 Main parameters extracted from the electrical measurements of the van der Pauw and TLM structures in graphene, contacted using Cr/Au (20/70 nm). The method used is explained in the SI. The data are averaged over several TLM structures. R_{SH} is the sheet resistance of graphene in the region between two metal contacts, R_{SK} is the sheet resistance of graphene under the metal contact, L_{TK} is the portion of the contact involved in conduction and ρ_C is the specific contact resistivity associated with the graphene–metal interface

Sample	R_{SH} [Ω sq^{-1}]	ρ_C [Ω cm^2]	L_{TK} [μm]	R_{SK} [kΩ]
G/a-SiN	810 ± 44	(2.0 ± 0.2) 10^4	1.8 ± 0.3	9.0 ± 1.4
G/SiO_2	843 ± 90	(1.6 ± 0.7) 10^4	3.1 ± 0.7	1.3 ± 0.5

metal contacts, electro–chemical interactions between graphene and metal are formed, determining the reduction of graphene charge and impacting the R_{SK} value. We can notice that for the a-SiN substrate, R_{SK} is 10 times larger than R_{SH}, while it only doubles for the SiO_2 substrate.

The first validation step involved Raman analysis of both types of samples used for electrical characterization: FLG on a transparent substrate (G/a-SiN) and on a conventional opaque substrate (G/SiO_2). The statistical analysis of the Raman spectra revealed that the substrate type (a-SiN or SiO_2/Si) does not significantly affect the Raman spectral parameters (peak positions and relative intensities). Representative spectra are shown in Fig. S4, and the corresponding spectral parameters are summarized in Table 2 (standard configuration with graphene on top). The only notable difference observed is a higher background signal in the a-SiN substrate.

The micro Raman maps were acquired on the same structures (TLM and VdP) previously measured simply by flipping the sample upside down. As shown in Fig. 1c and d, optimized thicknesses of the a-SiN and Al layers in the substrate enable the clear identification of the graphene layer under the optical microscope, both as a standalone film as well as in the presence of the metal contact. We can notice that the absolute intensity obtained for the Raman signal when graphene is on the bottom (device flipped upside down) was approximately reduced by one order of magnitude with respect to the conventional measurements with graphene on top (Fig. S4a). This reduction can be attributed to optical losses along the light path. Around 40% of the laser power is attenuated after transmission through the substrate (Fig. 1b), and an additional 40% attenuation affects the backscattered Raman signal, resulting in an overall attenuation of *c.a.* 16%, which aligns well with the experimental observations. Despite this decrease in absolute intensity, the relative peak intensities, positions, and full widths at half maximum (FWHM) remained virtually unchanged (Table 2) and were independent of the measurement direction. This outcome constitutes the second validation step, confirming the robustness of our approach for acquiring micro-Raman signals in the upside-down configuration, enabled by the specifically engineered transparent substrate.

Thus, considering the validity of our approach, we moved to compare the results obtained from the graphene and the graphene–metal interface. First, comparing the Raman measurements performed on graphene outside and under metal contact (Au/Cr/G/a-SiN) in VdP test structures, we obtained a reduced Raman signal-to-noise ratio for the latter.

Raman spectroscopy revealed an overall increase in the D band and a decrease in the 2D in the metallic contact area (Au/Cr/G/a-SiN) compared to pristine graphene. This general trend can be observed both from the comparison of individual spectra (Fig. 2a) as well as from combined data presented in histograms (Fig. 2b–2d) and from Raman maps (Fig. 3). This spectroscopic evidence supports the conclusion that the metallic contact (Cr) on top of graphene induces a significant amount of defects. An increase in defects is commonly observed in metal/graphene interfaces in the literature and depends on the metal used for contact and on the deposition technique.[26] In the specific case of Cr, an increase in the disorder was reported, even if it seems quite limited compared to Ti or other metals.[13] An increase in disorder in graphene has also been observed after the deposition of a dielectric layer on top of graphene, which is transparent to visible light and allows Raman spectroscopy to be performed after deposition. For instance, Al_2O_3 deposited by sputtering shows similar Raman results in terms of increased disorder, as indicated by the rise of the D band.[27] Similarly, an increase in disorder was reported after the encapsulation of graphene with Si_3N_4.[28] The broadening and decrease in the intensity of the 2D band have a less straightforward explanation. However, the literature suggests that a decrease in the 2D

Table 2 Raman spectral parameters extracted for graphene on oxide (G/SiO_2) and on transparent substrate (G/a-SiN) in top configuration (2nd and 3rd columns), and in upside down configuration (4th and 5th columns) without (G/a-SiN) and with top contacts (Au/Cr/G/a-SiN) for the VdP test structure

Raman configuration	Standard (G on top)		Upside down (G on bottom)	
Sample	G/SiO_2	G/a-SiN	G/a-SiN	Au/Cr/G/a-SiN
D/cm^{-1}	1367 ± 2	1371 ± 2	1368 ± 1	1363 ± 3
G/cm^{-1-1}	1589 ± 1	1589 ± 2	1587 ± 2	1583 ± 2
2D/cm^{-1}	2728 ± 3	2729 ± 4	2726 ± 5	2723 ± 5
D′/cm^{-1}	1625 ± 2	1625 ± 3	1625 ± 3	1620 ± 2
I_D/I_G	0.08 ± 0.03	0.08 ± 0.03	0.09 ± 0.03	0.39 ± 0.06
FWHM(2D)/cm^{-1}	41 ± 3	43 ± 4	45 ± 4	68 ± 10
I_{2D}/I_G	1.5 ± 0.5	1.2 ± 0.4	1.3 ± 0.4	0.5 ± 0.1

 © 2025 The Author(s). Published by the Royal Society of Chemistry

Open Access Article. Published on 05 November 2025. Downloaded on 1/22/2026 5:16:16 PM.
This article is licensed under a Creative Commons Attribution-NonCommercial 3.0 Unported Licence.

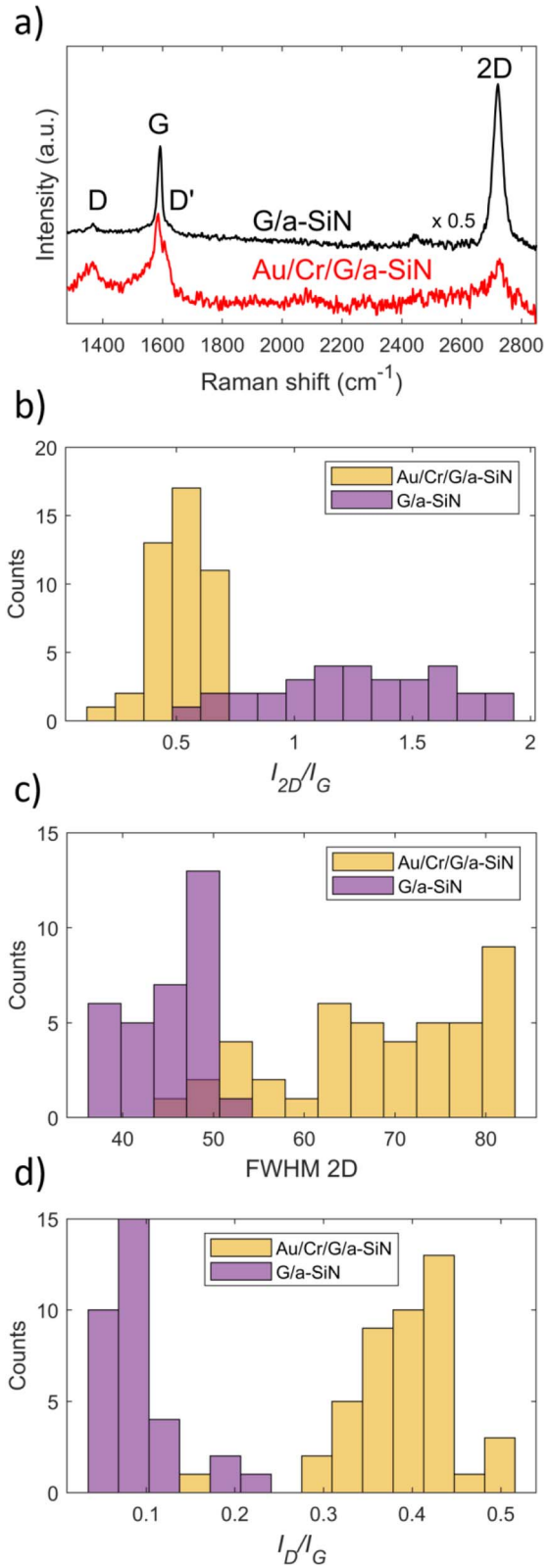

Fig. 2 (a) Representative Raman spectra of graphene with (Au/Cr/G/a-SiN curve) and without (G/a-SiN curve) metallic contact; histograms of (b) I_{2D}/I_G, (c) FWHM of 2D and (d) I_D/I_G for Au/Cr/G/a-SiN *vs.* G/a-SiN.

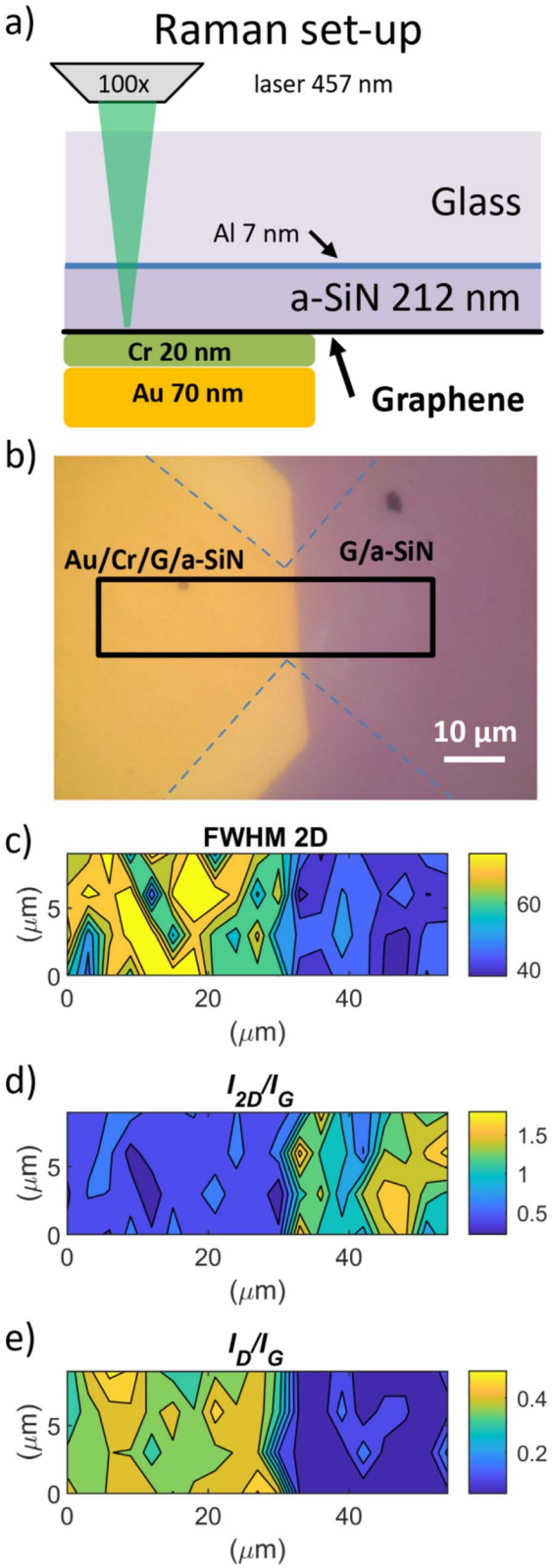

Fig. 3 (a) Scheme of the Raman measurement set-up for graphene on a transparent substrate in upside down configuration. (b) Micrograph of the VdP test structure with graphene under metallic contact (Au/Cr/G/a-SiN) at left and graphene without metallic contact (G/a-SiN) at right; the black rectangle represents the area of the sample probed by micro Raman. Raman maps of intensities of (c) FWHM for 2D signal, (d) I_{2D}/I_G and (e) I_D/I_G.

Open Access Article. Published on 05 November 2025. Downloaded on 1/22/2026 5:16:16 PM.
This article is licensed under a Creative Commons Attribution-NonCommercial 3.0 Unported Licence.

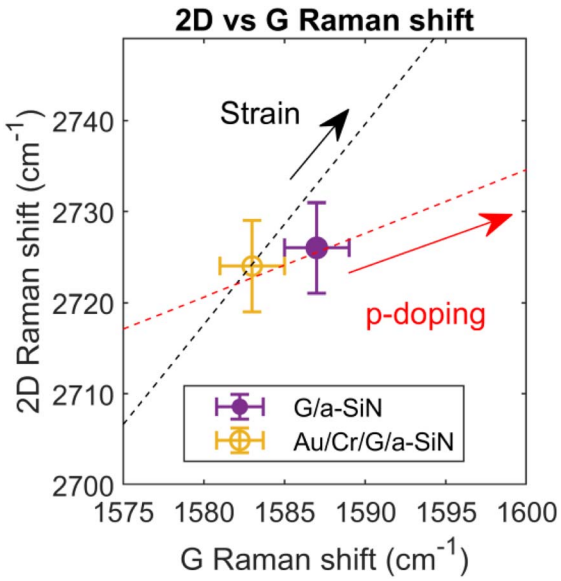

Fig. 4 Correlation analysis of 2D-G positions on G/a-SiN and Au/Cr/G/a-SiN. The dotted red line represents the direction of doping (slope 0.7), while the black dotted line represents the strain (slope 2.2).

band intensity relative to the G band occurs due to the interaction of graphene with metals, like for graphene on copper[29] or for graphene covered with a thin metallic film, only few nanometers thick.[12] In the present work, we observed a significant increase in the D signal due to an increase in defects and a decrease in the 2D band intensity, which could be associated with an increased electron-defect scattering rate. Furthermore, the broadening of the G band (FWHM of G from 26 cm^{-1} to >50 cm^{-1}) supports that the defect density related to the I_D/I_G ratio has a drastic shift from low defect concentration to high defect concentration.[30] The overall increase in defects is also confirmed by the rise in the D′ band.[31]

Only a minor relative shift of the G band was observed (Table 2 and 2D *vs.* G dispersions in Fig. 4), with no significant change in 2D peak position. This is partially in contrast to the findings reported for bottom contacts by Sakavičius,[17] where an increase in compressive strain was observed near the contact edges, with no increase in defects due to the bottom contact geometry, which avoids direct metal deposition on top of the graphene layer.

In the present work, no significant variation in strain due to contact was observed, while a slight decrease in p-doping occurred in graphene after the deposition of the metal. This is not in contrast with the main results reported in the literature for graphene/metal interfaces, with a few nanometers of metal deposited on top, where the G band presented in some cases a positive 10 cm^{-1} shift associated with an increase in graphene doping,[12] while in other cases, a negative shift of around 11 cm^{-1} was reported.[32] From our result, the decrease in doping due to G redshift is limited to few cm^{-1}.

The Raman maps obtained in the TLM area, where a 12 × 44 μm^2 area was probed on the device with 20 μm graphene channel width, with 6 μm width metal contacts (Fig. S5), reveal that the signals from the 3 contacts (5, 10, and 15 μm) exhibit the same characteristics as those obtained under the larger VdP contact (Fig. 3). This demonstrates that the approach presented here can be applied to study graphene locally under different metal contact configurations. In particular, the regions with and without metal can be distinguished using the Raman map of the FWHM of the 2D peak and the intensity ratio of the D and 2D peaks over the G signal (I_D/I_G and I_{2D}/I_G). The achieved resolution allows for the investigation of the single contact of a device. However, the overall spatial resolution in the Raman mapping using the upside down configuration presented in this work is >2 μm, while that obtained in the common set-up is <1 μm. The reduced resolution is due to internal reflections broadening the effective size of the laser spot on the sample.

Conclusion

In summary, the experimental approach developed to access the graphene–metal interface *via* Raman spectroscopy was successfully validated. Raman analysis performed on operating devices (TLM and VdP structures) revealed a significantly higher defect density at the graphene/metal interface (Au/Cr/G/a-SiN) compared to bare graphene, accompanied by a slight reduction in p-type doping. These findings are consistent with the observed increase in sheet resistance under metal, as obtained from the electrical characterization of linear TLM devices. The proposed technique also enables the investigation of the correlation between the amount of defects and contact resistance using various metals and/or different deposition techniques, offering a valuable tool for investigating the origin and mechanisms behind contact resistance. We acknowledge that the most accurate approaches for defect estimation involve techniques such as *C–V* sweeping and related methods. Nonetheless, in this study, we demonstrate that Raman spectroscopy can be effectively employed as a rapid and simple tool for evaluating the damage induced in the graphene layer during top metal contact fabrication. This assessment is performed by directly comparing Raman spectra collected on the same device in two distinct regions: bare graphene and graphene buried beneath the metal. The structural insights obtained in this way are further complemented with electrical measurements of the graphene/metal contact, including sheet resistance and contact resistance, thereby providing a comprehensive and integrated description of the system. Notably, the approach described can be extended to graphene directly grown on a transparent substrate, such as sapphire,[33] or to graphene transferred on any transparent substrate. Moreover, using this approach, Raman measurements can be performed simultaneously with electrical measurements, permitting the study of materials and devices under operating conditions that correlate structural properties (provided by Raman spectroscopy) with electrical properties in real time.[34] The method will be further implemented and verified using other metals (nickel, platinum and gold) for generalization.

Conflicts of interest

There are no conficts to declare.

 © 2025 The Author(s). Published by the Royal Society of Chemistry

Open Access Article. Published on 05 November 2025. Downloaded on 1/22/2026 5:16:16 PM.
This article is licensed under a Creative Commons Attribution-NonCommercial 3.0 Unported Licence.

Data availability

The data supporting this article have been included as part of the supplementary information (SI). Supplementary information: the Electrical Characterization, the Contact End Resistance (RCE) method and further Raman spectra are reported in the SI. See DOI: https://doi.org/10.1039/d5na00846h.

Acknowledgements

This research was partially funded by the project PNRR–M4C2INV1.5, NextGenerationEU call 3277/2021-ECS_00000033-ECOSISTER-spk001. The Raman spectrometer used in present work was funded by the project iENTRANCE@ENL: Infrastructure for Energy TRAnsition aNd Circular Economy @ Euro-NanoLab, Project Code: IR0000027, funded under the National Recovery and Resilience Plan (NRRP), Mission 04 Component 2 Investment 3.1–NextGenerationEU. The authors would like to thank Filippo Bonafé, Fabrizio Tamarri, Michele Sanmartin, Michele Bellettato, Giulio Pizzochero of CNR-ISMN Bologna (Italy) for their technical support in the fabrication of the graphene devices, and Dr Caterina Summonte for the support in preparing the transparent substrates. Preliminary Raman measurements were performed at the interdepartmental instrument facility at the University of Modena and Reggio Emilia (Centro Interdipartimentale Grandi Strumenti, UNIMORE), with the financial support of Prof. Francesco Rossella and the technical assistance of Jonathan Vinet, PhD.

References

1 F. Xia, V. Perebeinos, Y.-m. Lin, Y. Wu and P. Avouris, The origins and limits of metal–graphene junction resistance, *Nat. Nanotechnol.*, 2011, **6**(3), 179–184.
2 V. Sorianello, M. Midrio, G. Contestabile, I. Asselberghs, J. Van Campenhout, C. Huyghebaert, I. Goykhman, A. Ott, A. Ferrari and M. Romagnoli, Graphene–silicon phase modulators with gigahertz bandwidth, *Nat. Photonics*, 2018, **12**(1), 40–44.
3 F. Giubileo and A. Di Bartolomeo, The role of contact resistance in graphene field-effect devices, *Prog. Surf. Sci.*, 2017, **92**(3), 143–175.
4 A. Gahoi, S. Wagner, A. Bablich, S. Kataria, V. Passi and M. C. Lemme, Contact resistance study of various metal electrodes with CVD graphene, *Solid-State Electron.*, 2016, **125**, 234–239.
5 G. Giovannetti, P. A. Khomyakov, G. Brocks, V. M. Karpan, J. van den Brink and P. J. Kelly, Doping Graphene with Metal Contacts, *Phys. Rev. Lett.*, 2008, **101**(2), 026803.
6 S. M. Song, J. K. Park, O. J. Sul and B. J. Cho, Determination of Work Function of Graphene under a Metal Electrode and Its Role in Contact Resistance, *Nano Lett.*, 2012, **12**(8), 3887–3892.
7 J. A. Robinson, M. LaBella, M. Zhu, M. Hollander, R. Kasarda, Z. Hughes, K. Trumbull, R. Cavalero and D. Snyder, Contacting graphene, *Appl. Phys. Lett.*, 2011, **98**(5), 053103.
8 E. Watanabe, A. Conwill, D. Tsuya and Y. Koide, Low contact resistance metals for graphene based devices, *Diamond Relat. Mater.*, 2012, **24**, 171–174.
9 S. Min Song, T. Yong Kim, O. Jae Sul, W. Cheol Shin and B. Jin Cho, Improvement of graphene–metal contact resistance by introducing edge contacts at graphene under metal, *Appl. Phys. Lett.*, 2014, **104**(18), 183506.
10 C. Gong, S. McDonnell, X. Qin, A. Azcatl, H. Dong, Y. J. Chabal, K. Cho and R. M. Wallace, Realistic metal–graphene contact structures, *ACS Nano*, 2014, **8**(1), 642–649.
11 B. J. Schultz, C. Jaye, P. S. Lysaght, D. A. Fischer, D. Prendergast and S. Banerjee, On chemical bonding and electronic structure of graphene–metal contacts, *Chem. Sci.*, 2013, **4**(1), 494–502.
12 W. X. Wang, S. H. Liang, T. Yu, D. H. Li, Y. B. Li and X. F. Han, The study of interaction between graphene and metals by Raman spectroscopy, *J. Appl. Phys.*, 2011, **109**(7), 07C501.
13 M. W. Iqbal, A. K. Singh, M. Z. Iqbal and J. Eom, Raman fingerprint of doping due to metal adsorbates on graphene, *J. Phys.: Condens. Matter*, 2012, **24**(33), 335301.
14 H. Xu, X. Wu, X. Li, C. Luo, F. Liang, E. Orignac, J. Zhang and J. Chu, Properties of graphene-metal contacts probed by Raman spectroscopy, *Carbon*, 2018, **127**, 491–497.
15 W. S. Leong, H. Gong and J. T. Thong, Low-contact-resistance graphene devices with nickel-etched-graphene contacts, *ACS Nano*, 2014, **8**(1), 994–1001.
16 A. Sakavičius, G. Astromskas, A. Lukša, V. Bukauskas, V. Nargelienė, I. Matulaitienė and A. Šetkus, Annealing Time Effect on Metal Graphene Contact Properties, *ECS J. Solid State Sci. Technol.*, 2018, **7**(5), M77.
17 A. Sakavičius, G. Astromskas, V. Bukauskas, M. Kamarauskas, A. Lukša, V. Nargelienė, G. Niaura, I. Ignatjev, M. Treideris and A. Šetkus, Long distance distortions in the graphene near the edge of planar metal contacts, *Thin Solid Films*, 2020, **698**, 137850.
18 F. Fromm, P. Wehrfritz, M. Hundhausen and T. Seyller, Looking behind the scenes: Raman spectroscopy of top-gated epitaxial graphene through the substrate, *New J. Phys.*, 2013, **15**(11), 113006.
19 P. Blake, E. W. Hill, A. H. Castro Neto, K. S. Novoselov, D. Jiang, R. Yang, T. J. Booth and A. K. Geim, Making graphene visible, *Appl. Phys. Lett.*, 2007, **91**(6), 063124.
20 N. Bendiab, J. Renard, C. Schwarz, A. Reserbat-Plantey, L. Djevahirdjian, V. Bouchiat, J. Coraux and L. Marty, Unravelling external perturbation effects on the optical phonon response of graphene, *J. Raman Spectrosc.*, 2018, **49**(1), 130–145.
21 E. Centurioni, Generalized matrix method for calculation of internal light energy flux in mixed coherent and incoherent multilayers, *Appl. Opt.*, 2005, **44**(35), 7532–7539.
22 P. Maccagnani, *Integration in Silicon Microelectronic Technology*, Università di Ferrara, Ferrara, Italy, 2023 https://hdl.handle.net/11392/2506194.
23 S. Venica, F. Driussi, A. Gahoi, P. Palestri, M. C. Lemme and L. Selmi, On the adequacy of the transmission line model to

Open Access Article. Published on 05 November 2025. Downloaded on 1/22/2026 5:16:16 PM.
This article is licensed under a Creative Commons Attribution-NonCommercial 3.0 Unported Licence.

describe the graphene–metal contact resistance, *IEEE Trans. Electron Devices*, 2018, **65**(4), 1589–1596.

24 A. J. Pollard, K. R. Paton, C. A. Clifford, and E. Legge, *Characterisation of the Structure of Graphene, Good Practice Guide*, National Physical Laboratory, UK, 2017.

25 G. Reeves and H. Harrison, Obtaining the specific contact resistance from transmission line model measurements, *IEEE Electron Device Lett.*, 1982, **3**(5), 111–113.

26 W. J. Liu, H. Y. Yu, J. Wei and M. F. Li, Impact of Process Induced Defects on the Contact Characteristics of Ti/Graphene Devices, *Electrochem. Solid-State Lett.*, 2011, **14**(12), K67.

27 M. Friedemann, M. Woszczyna, A. Müller, S. Wundrack, T. Dziomba, T. Weimann and F. J. Ahlers, Versatile sputtering technology for Al2O3 gate insulators on graphene, *Sci. Technol. Adv. Mater.*, 2012, **13**(2), 025007.

28 M. A. Giambra, V. Mišeikis, S. Pezzini, S. Marconi, A. Montanaro, F. Fabbri, V. Sorianello, A. C. Ferrari, C. Coletti and M. Romagnoli, Wafer-scale integration of graphene-based photonic devices, *ACS Nano*, 2021, **15**(2), 3171–3187.

29 O. De Luca, R. Grillo, M. Castriota, A. Policicchio, M. P. De Santo, G. Desiderio, A. Fasanella, R. G. Agostino, E. Cazzanelli, M. Giarola and G. Mariotto, Different spectroscopic behavior of coupled and freestanding monolayer graphene deposited by CVD on Cu foil, *Appl. Surf. Sci.*, 2018, **458**, 580–585.

30 A. Eckmann, A. Felten, I. Verzhbitskiy, R. Davey and C. Casiraghi, Raman study on defective graphene: Effect of the excitation energy, type, and amount of defects, *Phys. Rev. B:Condens. Matter Mater. Phys.*, 2013, **88**(3), 035426.

31 F. Tuinstra and J. L. Koenig, Raman spectrum of graphite, *J. Chem. Phys.*, 1970, **53**(3), 1126–1130.

32 I. Serrano-Esparza, J. Fan, J. M. Michalik, L. A. Rodríguez, M. R. Ibarra and J. M. de Teresa, The nature of graphene–metal bonding probed by Raman spectroscopy: the special case of cobalt, *J. Phys. D: Appl. Phys.*, 2016, **49**(10), 105301.

33 N. Mishra, S. Forti, F. Fabbri, L. Martini, C. McAleese, B. R. Conran, P. R. Whelan, A. Shivayogimath, B. S. Jessen, L. Buß, J. Falta, I. Aliaj, S. Roddaro, J. I. Flege, P. Bøggild, K. B. K. Teo and C. Coletti, Wafer-scale synthesis of graphene on sapphire: toward fab-compatible graphene, *Small*, 2019, **15**(50), 1904906.

34 P. Vecera, S. Eigler, M. Koleśnik-Gray, V. Krstić, A. Vierck, J. Maultzsch, R. A. Schäfer, F. Hauke and A. Hirsch, Degree of functionalisation dependence of individual Raman intensities in covalent graphene derivatives, *Sci. Rep.*, 2017, **7**(1), 45165.

 © 2025 The Author(s). Published by the Royal Society of Chemistry